Influence of deepening and mesoscale organization of shallow convection on stratiform cloudiness in the downstream trades

Raphaela Vogel, Louise Nuijens, Bjorn Stevens

Received: 15 May 2019 | Revised: 18 August 2019 | Accepted: 13 September 2019

DOI: 10.1002/qj.3664

RESEARCH ARTICLE

Quarterly Journal of the Royal Meteorological Society RMetS

Influence of deepening and mesoscale organization of shallow convection on stratiform cloudiness in the downstream trades

Raphaela Vogel[2] | Louise Nuijens[3] | Bjorn Stevens[1]

[1]Max Planck Institute for Meteorology, Hamburg, Germany

[2]LMD/IPSL, CNRS, Sorbonne University, Paris, France

[3]Department of Geosciences and Remote Sensing, Delft University of Technology, Delft, The Netherlands

Correspondence
Raphaela Vogel, LMD/IPSL, Sorbonne University, case 99, 4 Place Jussieu, 75252 Paris cedex 05, France
Email: raphaela.vogel@lmd.jussieu.fr

Present address Raphaela Vogel, LMD/IPSL, Sorbonne University, case 99, 4 Place Jussieu, 75252 Paris cedex 05, France.

Funding information
Max Kade Foundation Postdoctoral Research Grant; Reimar Luest Stipendium

Abstract

In this study we use large-eddy simulation to explore the factors controlling stratiform cloudiness in the downstream trades. We perform sensitivity experiments with different large-scale forcings, radiation specifications and domain sizes, which isolate the influence of convective deepening, moisture–radiation interactions and mesoscale organization, respectively. Across the simulations with different large-scale forcings, we find that the deepening of the cloud layer and the associated increase in precipitation strongly correlate with decreasing inversion strength and stratiform cloudiness. The relationship between cloud-layer depth and cloud amount is largely independent of the way a specific change in the large-scale forcing induces the deepening. The interaction of radiation with the domain-averaged humidity and cloud profile is necessary for stratiform cloudiness to form. Strong radiative cooling experienced by updraughts overshooting a strong inversion induces the formation of detrained stratiform layers, and strong long-wave cooling associated with the stratiform layers stabilizes the inversion. Interactive radiation is also important for exposing differences in shallow convection under different free-tropospheric humidities. A drier initial free troposphere leads to both increased cloud-layer and free-tropospheric radiative cooling and increased surface evaporation, which forces deeper convection and more precipitation compared to a moister initial free troposphere. The simulations with a drier initial free troposphere thus have weaker inversions and less stratiform cloud. The organization of convection into larger clusters in large-domain simulations increases precipitation and weakens the inversion compared to a simulation on a 16-fold smaller domain, which does not support convective organization. Organized updraught clusters carry more moisture and liquid to the inversion, so that the same amount of stratiform cloudiness forms, despite the inversion being weaker. The simulations presented here suggest that the deepening and organization of shallow convection plays an important role in regulating stratiform cloudiness and thus total cloud cover in the downstream trades.

KEYWORDS

large-eddy simulation, mesoscale organization, moisture–radiation interactions, shallow convection, stratiform cloudiness

1 INTRODUCTION

Shallow trade cumulus clouds are a dominant cause of spread in projections of future climate (e.g. Bony and Dufresne, 2005; Boucher *et al.*, 2013; Vial *et al.*, 2013). Contributions to low cloud cover in the trades stem from two important height levels, near the lifting condensation level and near the trade-inversion (Nuijens *et al.*, 2014). Observations from the Barbados Cloud Observatory, which are representative for conditions across the broader trades (Medeiros and Nuijens, 2016), indicate that one-third of low cloud cover and two-thirds of its variability are due to cloudiness near the trade inversion (Nuijens *et al.*, 2014; 2015b). Cloudiness near the inversion is either due to the presence of stratiform cloud layers near cumulus tops, sheared deeper trade cumulus or passive remnants of decaying clouds, and its larger coverage in winter accounts for the larger cloud cover of this season (Nuijens *et al.*, 2014; 2015b). Previous studies using large-eddy simulation (LES) showed that stronger inversions tend to increase stratiform cloudiness near cumulus tops, and that precipitation and the deepening of convection tends to decrease stratiform cloudiness (Wyant *et al.*, 1997; Stevens *et al.*, 1998; 2001; Lock, 2009). However, these studies focused on stratocumulus or very shallow trade-wind layers more representative of the stratocumulus-to-cumulus transition, and it is unclear whether the understanding applies to the deeper trade-wind layers found over warmer waters further downstream.

Namely, at Barbados, stratiform cloud layers are generally absent during more suppressed periods with very shallow cumuli – conditions often associated with the Barbados Oceanographic and Meteorological Experiment field campaign (BOMEX: Siebesma *et al.*, 2003). Instead, stratiform layers are frequent in the presence of deeper cumuli or cumulus congestus with tops between 2.5 and 4.5 km, which tend to be clustered and are reminiscent of the *cloud flowers pattern* seen in satellite imagery (see Fig. 4 in Stevens *et al.*, 2019). For the downstream trades, it has been difficult to link the mean inversion strength to cloud cover in observations, and correlations of inversion cloudiness with large-scale factors like subsidence or wind speed are also generally weak on time-scales shorter than a month (Brueck *et al.*, 2015; Nuijens *et al.*, 2015b). This raises the question as to the cloud-controlling factors, including the deepening and organization of shallow convection, and moisture–radiation interactions, in determining inversion strength and stratiform cloudiness in the downstream trades.

Observational studies indicate that stratiform layers tend to become thinner as clouds get deeper (Lamer *et al.*, 2015; O *et al.*, 2018). O *et al.* (2018) attribute this to increased precipitation scavenging with increasing cloud depth, which strongly reduces the cloud droplet number concentration in the detrained stratiform layers. Wyant *et al.* (1997) showed that when convection deepens and penetrates the inversion, the upper cloud layer dries due to enhanced penetrative entrainment, and stratiform layers go away.

In a previous modelling study we showed that the spontaneous organization of shallow convection into deeper and larger precipitating clusters in large-domain LES leads to a shallower, warmer and drier domain-average trade-wind layer compared to a simulation on a 16-fold smaller domain without organization (Vogel *et al.*, 2016). The organization of convection strongly enhances the moisture variance in the cloud layer, as convecting regions become moister compared to small-domain simulations without organization, even if the domain-averaged humidity reduces through disproportionate drying of the clear-sky regions (Seifert and Heus, 2013; Vogel *et al.*, 2016). Because updraughts carry more moisture to the inversion, stratiform cloud layers may form more readily when shallow convection is organized.

The interaction of radiation with water vapour and cloud droplets is another important factor influencing stratiform cloudiness near cumulus tops (Stevens *et al.*, 2001; Lock, 2009). Strong long-wave cooling at cloud tops under strong inversions constitutes a positive radiative feedback, increasing stratiform cloud amount in the LES intercomparison of the Atlantic Tradewind Experiment case (ATEX: Stevens *et al.*, 2001). Interactive radiation is also important for the evolution of the trade-wind layer and for cloud depth, as it destabilizes the cloud layer and leads to more active convection in LES (Seifert *et al.*, 2015).

Motivated by these past studies and insights, this article addresses the following questions: How do the deepening and organization of shallow convection, under somewhat different large-scale forcings and for different domain sizes, influence the inversion structure and stratiform cloudiness? And what is the role of moisture–radiation interactions therein? We perform LES with a model domain of $51.2 \times 51.2 \times 10$ km^3, which was shown to be large enough to support the mesoscale organization of shallow convection and the emergence of deeper congestus clouds (e.g. Seifert and Heus, 2013; Vogel *et al.*, 2016). Note that we do not quantify the degree of mesoscale organization here, but simply examine whether clouds are clustered in visual snapshots, and whether the moisture variance is large. The trade-wind layer in the downstream trades extends to a depth of 1.5 to 3 km and is usually capped by a sharp decrease in humidity, sometimes called a hydrolapse. Throughout the article we use the term inversion to refer to this feature that is evident in both temperature and humidity.

We address the influence of the deepening of convection on the stratiform cloudiness in section 3 by varying the initial free-tropospheric humidity profile, wind speed, subsidence and sea-surface temperature (SST). The influence of moisture–radiation interactions is studied in section 4 by contrasting the simulations with the different initial

free-tropospheric humidity profiles under (a) fully interactive, (b) horizontally homogenized, and (c) prescribed uniform radiation. The influence of mesoscale organization is studied in section 5 by a comparison with a simulation on a 16-fold smaller domain. Conclusions are presented in section 6.

2 | LARGE-EDDY SIMULATION FRAMEWORK AND EXPERIMENTS

2.1 | LES framework

All the simulations are performed with the University of California Los Angeles (UCLA) LES (Stevens *et al.*, 2005), in a similar set-up as in Vogel *et al.* (2016). The UCLA LES solves the Ogura–Phillips anelastic equations using fourth-order centred differences and applies the Smagorinsky–Lilly model for the subgrid-scale fluxes. Prognostic equations are solved for the three wind components and the two thermodynamic variables total water mixing ratio q_t and liquid water potential temperature θ_l. Time-stepping is performed with a third-order Runge–Kutta integration. Liquid water is diagnosed with a saturation-adjustment scheme. Microphysical processes are based on the two-moment warm rain scheme of Seifert and Beheng (2001; 2006), as described in Savic-Jovcic and Stevens (2008). A constant cloud droplet number concentration $N_c = 50\,\mathrm{cm}^{-3}$ is assumed. Ice microphysical processes are not considered.

The large-scale thermodynamic state is based on an idealized representation of the conditions in the downstream trades, adapted from Bellon and Stevens (2012). The set-up uses a Eulerian reference frame and prescribes homogeneous large-scale forcings. The forcings include an exponential subsidence profile

$$w(z) = -w_0(1 - \mathrm{e}^{-z/H_w}), \tag{1}$$

where $w(z)$ is the subsidence rate at height z, w_0 is the prescribed base subsidence rate serving as the asymptotic value at high altitude (default value $w_0 = 7.5\,\mathrm{mm{\cdot}s^{-1}}$), and $H_w = 1$ km is the scale height. The resulting heating and moistening tendencies due to subsidence are computed at each time step and grid point by multiplying $w(z)$ by the local vertical gradient of θ_l and q_t.

Similar to the standard configuration of Bellon and Stevens (2012), the free-tropospheric temperature lapse rate follows from the balance of a prescribed uniform radiative heating tendency, $Q_R = -2.5\ \mathrm{K{\cdot}day^{-1}}$, and the subsidence rate $w(z)$ as

$$\frac{d\theta_l}{dz} = \frac{Q_R}{w(z)}. \tag{2}$$

The surface fluxes are modelled using bulk aerodynamic formulae, with fixed SSTs and a slip/no-penetration condition. A constant geostrophic zonal wind u_g is imposed, with a default value of $10\ \mathrm{m{\cdot}s^{-1}}$. No horizontal advective cooling and drying tendencies are applied.

Except for the sensitivity experiments testing the influence of the radiation treatment (see section 2.2 for details), the radiative heating tendency is computed interactively. Monte Carlo Spectral Integration (Pincus and Stevens, 2009) is used to compute the radiative fluxes based on the broadband radiation code of Fu and Liou (1992), similar to the implementation of Seifert *et al.* (2015). The radiative tendencies are computed for every column independently, depending on the specific profile of water vapour, temperature and liquid water. The profiles are blended to typical tropical profiles from the domain top at 10 km to the top of the atmosphere. A fixed solar zenith angle of 15° is used for the short-wave component. A prescribed uniform radiative cooling of $2.5\ \mathrm{K{\cdot}day^{-1}}$ is used during the first simulation hour so as to avoid drift in the simulations during their spin-up.

A grid spacing of 50 m in the horizontal and 10 m in the vertical is used, with the vertical grid uniformly stretched by a factor of 1.02. The simulations are performed on a $51.2 \times 51.2 \times 10\ \mathrm{km}^3$ domain ($1{,}024 \times 1{,}024 \times 155$ grid points), with doubly-periodic lateral boundary conditions.

2.2 | Numerical experiments

Table 1 provides an overview of the different simulations performed. We use two different initial free-tropospheric humidity profiles, a moist profile (denoted WET) and a dry profile (denoted DRY), with the latter being on average 1–1.5 $\mathrm{g{\cdot}kg^{-1}}$ drier. Both profiles have the same boundary-layer humidity, but use a different scale height for the exponential free-tropospheric profile

$$q_{t,ft}(z) = q_0 \mathrm{e}^{-z/H_q}, \tag{3}$$

where $q_0 = 4\ \mathrm{g\,kg^{-1}}$, $H_q = 5$ km for the WET profile and $H_q = 2$ km for the DRY profile. The *WET* and *DRY* simulations serve as a baseline for the other simulations. The simulations denoted with a "*" in the last column of Table 1 are restarted from these baseline simulations after 72 h, when the trade-wind layer is well developed (not shown).

We perform four simulations that address the influence of large-scale forcing factors other than the free-tropospheric humidity. The influence of wind speed is explored by increasing the zonal geostrophic wind u_g from 10 to $15\ \mathrm{m{\cdot}s^{-1}}$ in the *WET.u15* and *DRY.u15* cases. The influence of large-scale subsidence is studied by increasing the prescribed base subsidence rate w_0 to $8.5\ \mathrm{mm{\cdot}s^{-1}}$ in the *DRY.ω8.5* case. Finally, the influence of SST is studied by a 2 K increase in SST to 302 K in the *WET.2K* case.

To study the influence of radiation on the stratiform cloudiness, three additional simulations are performed. The *WET.unirad* and *DRY.unirad* simulations use a prescribed

TABLE 1 Specifications used for the different experiments

Case name	q_t prof. [−]	u_g [m·s^{-1}]	ω_0 [mm·s^{-1}]	SST [K]	Radiation [−]	Domain [km^2]	Analysis interval [day]
WET	WET	10	7.5	300	Interactive	51.2×51.2	3.5–5.5
DRY	DRY	10	7.5	300	Interactive	51.2×51.2	3–5
WET.u15	WET	15	7.5	300	Interactive	51.2×51.2	4–6*
DRY.u15	DRY	15	7.5	300	Interactive	51.2×51.2	4–6*
Dry.ω8.5	DRY	10	8.5	300	Interactive	51.2×51.2	4–6*
WET.2K	WET	10	7.5	302	Interactive	51.2×51.2	5.5–7.5*
DRY.unirad	DRY	10	7.5	300	Uniform	51.2×51.2	2.5–4
WET.unirad	WET	10	7.5	300	Uniform	51.2×51.2	2.5–4.5
WET.homrad	WET	10	7.5	300	Homogenized	51.2×51.2	3.5–5.5*
WET.small	WET	10	7.5	300	Interactive	12.8×12.8	3.5–5.5

Free-tropospheric humidity profile, geostrophic wind component u_g, base subsidence rate ω_0, SST, radiation treatment, domain size, and analysis interval of statistics. "*" refers to simulations that have been perturbed after 3 days from the baseline simulation with the same initial humidity profile.

uniform radiative heating tendency of −2.5 K·day^{-1}. For the *WET.homrad* simulation, both the long-wave and short-wave radiative heating tendencies are homogenized horizontally at each time step and height level, such that local interactions between convection and radiation are inhibited. The sensitivity to the organization of shallow convection is tested in the *WET. small* simulation, which uses a 16-fold smaller horizontal domain size (12.8 × 12.8 km^2) that does not support the emergence of larger clusters (see Vogel *et al.*, 2016).

We perform all the simulations for several days and analyse the simulations in a quasi-stationary state (see the last column of Table 1 for the analysis interval used).

3 | RESPONSE OF INVERSION STRENGTH AND STRATIFORM CLOUDINESS TO THE DEEPENING OF CONVECTION

In this section, we examine how the deepening of shallow convection in response to varying large-scale forcings influences the inversion strength and the formation of stratiform layers. All simulations presented in Figure 1 and Table 2 use interactive radiation and are performed on the large 51.2 × 51.2 km^2 domain that supports mesoscale organization.

Figure 1a shows that the *WET* case with the moist initial free troposphere has a shallow and strong trade inversion (defined respectively as the height and magnitude of maximum stability). The cloud profile of the *WET* case shows a pronounced secondary cloud fraction maximum, which peaks at the base of this inversion and corresponds to the stratiform cloud layers. Figure 1 also displays profiles of other simulations with different free-tropospheric humidity, wind speed, subsidence and SST. Across these different simulations, the deepening of the cloud layer goes along with a weakening of

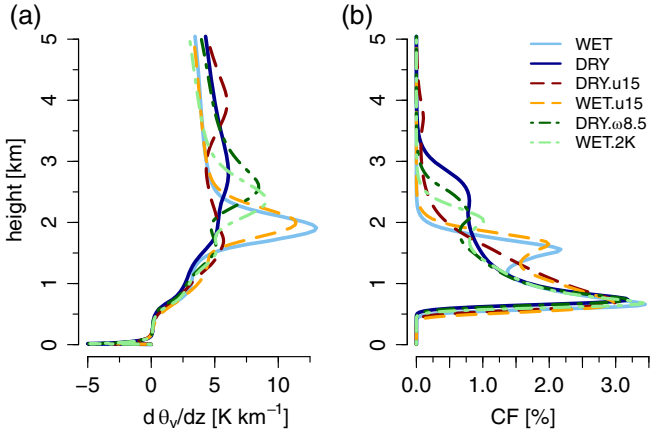

FIGURE 1 Domain-averaged profiles of (a) stability and (b) cloud fraction for the *WET*, the *DRY*, the *DRY.u15*, the *WET.u15*, the *DRY.ω8.5*, and the *WET.2K* simulations

the inversion and a decrease in stratiform cloudiness (see also Table 2). In contrast, cloudiness near the base of the cumulus layer at ∼700 m is largely insensitive to the forcing changes and the convective deepening (Nuijens *et al.*, 2014; 2015a; Vogel *et al.*, 2016).

The rate at which the cloud layer deepens is influenced by a number of factors. For example, prescribing a drier initial free troposphere in the *DRY* case deepens the cloud layer by 46% compared to the *WET* case, an effect we attribute to enhanced radiative cooling (due to the more transparent free troposphere) and to enhanced surface evaporation (due to stronger entrainment drying across the trade inversion); while increasing the SST by 2 K in the *WET.2K* case deepens the cloud layer by 24% compared to the *WET* case by increasing the surface fluxes and warming the cloud layer. Nevertheless, how the deepening of the cloud layer is induced does not seem to matter much for the inversion strength and stratiform

TABLE 2 Averages of the surface latent-heat flux (LHF), surface sensible-heat flux (SHF), surface buoyancy flux (SBF), surface precipitation rate (R_{surf}), inversion height and inversion strength (z_{inv} and $\Delta\theta_{v,\,inv}$, defined respectively as the height and magnitude of maximum stability), maximum cloud-top height (CTH_{max}), cloud cover (CC), the maxima of cloud fraction at cloud-base (CF_{base}), the inversion cloud fraction (CF_{inv}, defined as the cloud fraction maximum within 400 m below z_{inv}), liquid water path (LWP) and albedo (α, computed following Zhang *et al.* (2005) using $\alpha = \tau/(6.8+\tau)$, with an optical depth estimate of $\tau = 0.19\,\mathrm{LWP}^{5/6}\,N_c^{1/3}$), for the simulations with different large-scale forcings

Case name	LHF [W·m^{-2}]	SHF [W·m^{-2}]	SBF [cm^2·s^{-3}]	R_{surf} [W·m^{-2}]	z_{inv} [m]	$\Delta\theta_{v,\,inv}$ [K·km^{-1}]	CTH_{max} [m]	CC [%]	CF_{base} [g·m^{-2}]	CF_{inv} [%]	LWP [%]	α [%]
WET	205	1.2	4.79	11.1	1963	13.4	2,408	11.2	3.4	2.4	8.53	5.81
DRY	238	2.3	5.84	26.1	2,866	6.4	3,818	9.3	3.2	0.9	9.95	5.18
WET.u15	231	−3.1	4.09	21.3	2040	11.8	2,499	11.4	3.0	2.3	10.13	6.29
DRY.u15	258	−3.1	4.70	33.8	3,013	6.4	3,711	9.9	3.0	0.9	10.14	5.58
Dry.ω8.5	237	2.1	5.74	19.5	2,720	9.0	3,191	9.1	3.2	0.9	8.22	4.93
WET.2K	238	1.0	5.43	17.8	2,439	9.5	2,991	9.9	3.4	1.2	8.72	5.33

cloudiness. What seems to matter most is the amount of deepening that a forcing change induces.

With the deepening of the cloud layer, precipitation increases (see Table 2). The increased precipitation reduces evaporation at cloud tops and thus local evaporative cooling that otherwise helps strengthen the inversion. Also, the convective moisture source Q_2 (Yanai *et al.*, 1973) indicates a broader distribution of detrainment levels when convection is deeper (not shown). Further, the smoother humidity structure and the absence of stratiform cloud distributes the region of enhanced radiative cooling near the inversion (as discussed in the next section). These are reasons why the deepening of convection is related to the weakening of the inversion.

The simulation with most stratiform cloud and the simulation with least stratiform cloud in Figure 1 are the *WET* and the *DRY* case, which only differ in the initial free-tropospheric humidity profile. They are discussed in more detail in the next section, which focuses on moisture–radiation interactions.

4 | THE ROLE OF MOISTURE–RADIATION INTERACTIONS

4.1 | Influence of the free-tropospheric humidity profile

Figure 2 shows time series of the cloud fraction and radiative cooling profiles for the first 2.75 days of the *WET* case. The cloud layer progressively deepens during the first day. After about 20 h, intermittent features of high cloud fraction – the stratiform cloud layers – become apparent near 2 km. The stratiform cloud layers form when deeper congestus clouds develop, whose tops reach up to 3.5–4.5 km, and which produce substantial precipitation. The stratiform layers are accompanied by a peak in radiative cooling.

The spatial structure of the cloud field at one of those times is illustrated in Figure 3a–c, which display horizontal

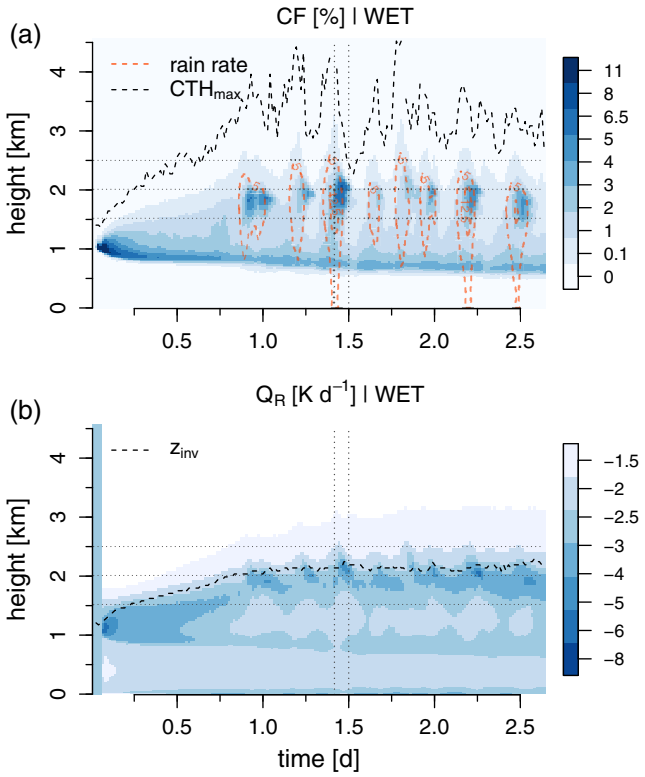

FIGURE 2 Temporal evolution of domain-averaged profiles of (a) cloud fraction and (b) radiative heating tendency Q_R for the *WET* case. The contour lines in (a) represent the precipitation amount in intervals of 5, 12.5 and 20 mg·kg^{-1}. Furthermore, the maximum cloud-top height and the inversion height are indicated in (a) and (b), respectively. Horizontal and vertical reference lines are added to facilitate the comparison of different features

cross-sections of cloud-top height during the 2 h period indicated by the dotted reference lines in Figure 2. At the initial stage of the stratiform cloudiness (Figure 3a), a large cluster of updraughts with turrets reaching up to 4 km is apparent. The 100–300 m thin stratiform layer forms in the vicinity of the large cloud cluster. While the deep updraughts have disappeared 40 min later (Figure 3b), the stratiform layer expands

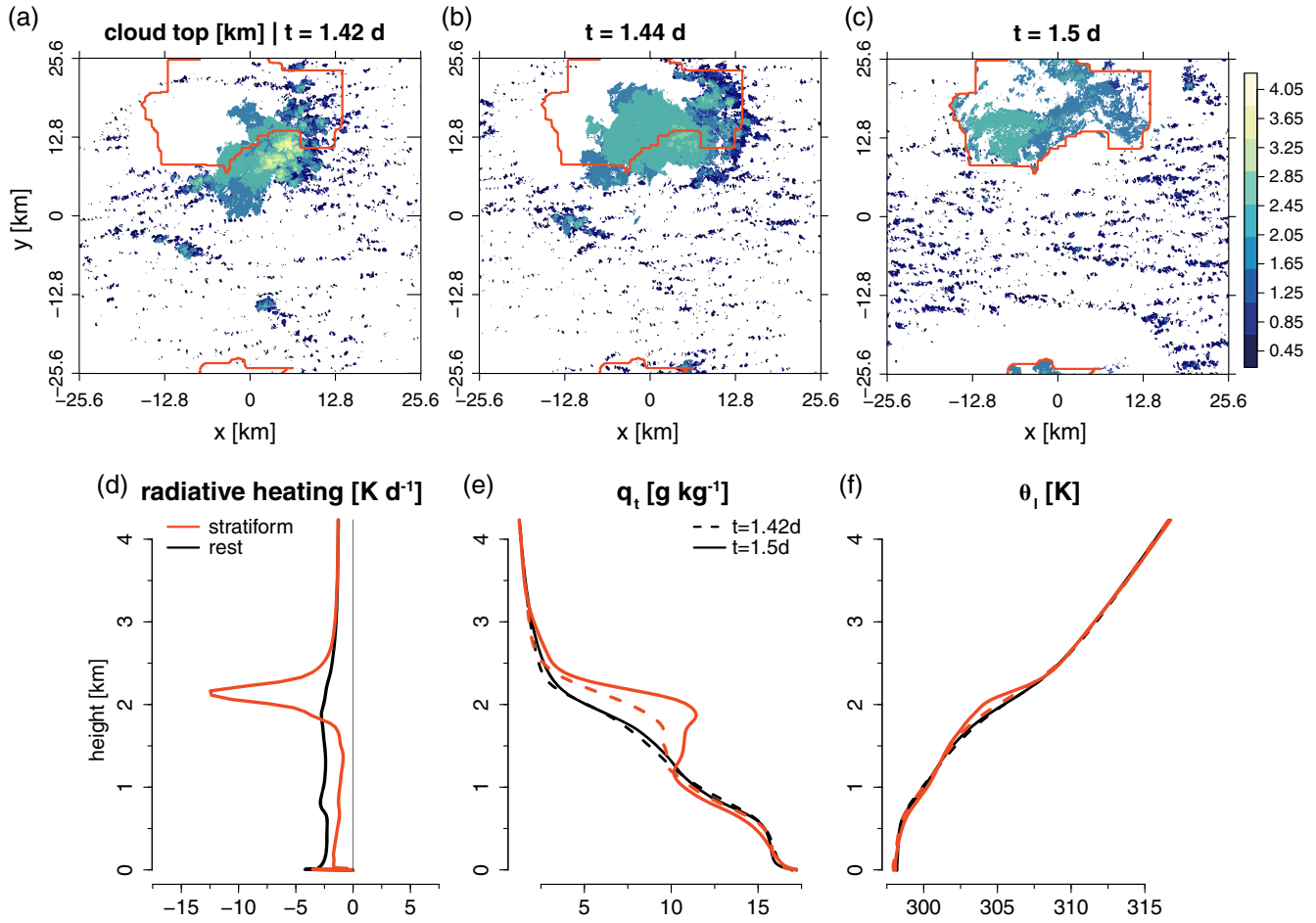

FIGURE 3 (a–c) Horizontal cross-sections of cloud-top height for the *WET* case at three times separated by 40 and 80 min, respectively. Profiles of (d) radiative heating tendency averaged over the 2 h interval shown in the cross-sections, and (e) humidity and (f) temperature at $t = 1.42$ days and $t = 1.5$ days, respectively. The profiles are conditioned on the area with stratiform cloud at $t = 1.5$ days as outlined in the cross-sections, and the rest of the domain

and spreads over the cold pool initiated by the cluster. The cool and dry air inside the cold pool suppresses surface-forced convection after about an hour (not shown). The lack of further moisture transport to the stratiform layer eventually leads to its dissipation after about 2 h. The simulated cloud structure is reminiscent of the *cloud flowers pattern* seen in satellite imagery (see Fig. 4 in Stevens *et al.*, 2019), but on a two to fivefold smaller scale.

Figure 3d contrasts the radiative heating tendencies in the region where the stratiform cloudiness occurs (indicated by the solid outline in the cross-sections, see the caption for details), and in the rest of the domain. The profiles demonstrate that very strong radiative cooling takes place near the inversion in the stratiform region, whereas radiative cooling in the lower cloud layer and sub-cloud layer is less than in the rest of the domain. Together with the strong evaporative cooling (not shown), this leads to a strengthening of the inversion jumps in temperature and humidity near 2 km in the stratiform region (Figure 3e,f).

In summary, the transport of moisture to the inversion by the large updraught cluster initiates the stratiform cloud layer, and the associated radiative and evaporative cooling locally strengthen the inversion. A stronger inversion prevents subsequent clusters from penetrating the inversion and maintains conditions favourable for stratiform cloudiness.

The importance of a strong inversion for the development of stratiform layers is evident for the *DRY* case. While stratiform layers form during the second day of the *DRY* case (Figure 4a), the progressive deepening of the cloud layer weakens the inversion and inhibits stratiform cloudiness after the second day. The drier free troposphere in the *DRY* case enhances radiative cooling in the cloud layer and the free troposphere compared to the *WET* case from the very beginning of the simulation (compare Figures 2b and 4b). The greater destabilization in the *DRY* case allows the deepest cumuli to penetrate more deeply. Deeper convection implies mixing of drier air to the surface, which enhances surface evaporation (see Table 3), and deepens convection further. Apparently, the lateral entrainment of drier air is not strong enough to counteract these effects (e.g. Bretherton *et al.*, 2004; Grabowski and Moncrieff, 2004).

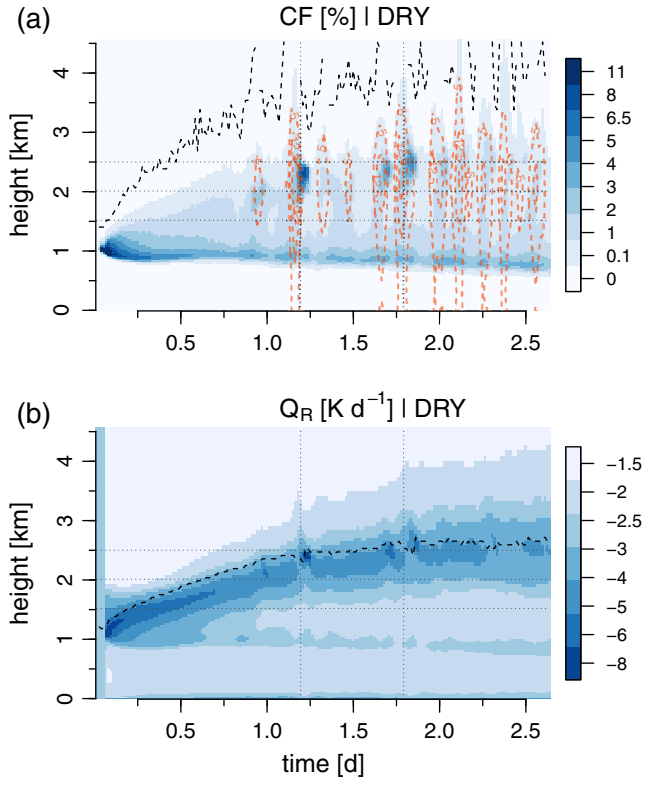

FIGURE 4 Same as Figure 2, but for the *DRY* case

4.2 | Radiation specification

The strong influence of moisture–radiation interactions on stratiform cloudiness becomes apparent when comparing the interactive radiation simulations (*WET* and *DRY*) to simulations performed with a uniform prescribed radiative cooling of −2.5 K·day^{-1} (*WET.unirad* and *DRY.unirad*). The profiles in Figure 5 show that with uniform radiation, the two simulations develop cloud tops and a cloud fraction profile that are more similar. Compared to the radiative heating profile of the interactive radiation cases, the cloud layer in the uniform radiation cases experiences less radiative cooling and the free troposphere experiences more radiative cooling (Figure 5b). More destabilization leads to deeper clouds in the uniform radiation cases (see Table 3). With deeper clouds and in the absence of a gradient in radiative cooling across the inversion, the *WET.unirad* case has a much weaker inversion than the *WET* case, and no stratiform layers develop. Note that the interactive radiation simulations develop a free-tropospheric heating surplus (Figure 5c), which helps stabilize the inversion in the *WET* case.

To test whether local radiation interactions are necessary for stratiform cloudiness to form, we horizontally homogenize the radiative cooling tendency at every time step and height level in the *WET.homrad* case, to retain only the interaction of radiation with the domain-averaged humidity, temperature and cloud profile. Figure 5a shows that the *WET.homrad* case has even more stratiform cloudiness compared to the *WET* case with fully interactive radiation. Also, a simulation that prescribes the near-equilibrium radiative cooling profile of the *WET* case develops stratiform layers comparable to the *WET* case (not shown). Apparently, the cooling does not necessarily need to be as strong and localized as in Figure 3d to form stratiform cloudiness. That homogenizing radiation can lead to even more stratiform cloudiness is somewhat surprising, but may be explained by the fact that the broad clear-sky areas surrounding the stratiform layers will cool more when radiation is homogenized, which can facilitate cloud formation there.

In summary, the results presented in this section show that large updraught clusters detraining under a strong inversion promote stratiform cloudiness and stabilize the inversion. The interaction of radiation with the (domain-averaged) humidity and cloud profile is crucial for developing a strong inversion and forming stratiform cloudiness.

5 | SENSITIVITY TO DOMAIN SIZE

The simulations discussed in the previous sections were all performed on a 51.2 × 51.2 km^2 domain that is large enough to support the mesoscale organization of shallow convection into larger and deeper cloud clusters (Seifert and Heus, 2013; Vogel *et al.*, 2016). To study the influence of the organization on the stratiform cloudiness, we perform a simulation with the same set-up as the *WET* case, but on a 16-fold smaller domain (12.8 × 12.8 km^2, *WET.small*).

The sequence of cloud-top height cross-sections in Figure 6 shows that the cloud field in the *WET.small* case is less clustered compared to the *WET* case (see Figure 3a–c). The *WET.small* case also has a much smaller moisture variance in the cloud layer (Figure 7a). The absence of mesoscale organization in the *WET.small* case has a strong influence on

TABLE 3 As Table 2, but for the simulations with different radiation and domain size specifications

Case name	LHF [W·m^{-2}]	SHF [W·m^{-2}]	SBF [cm^2·s^{-3}]	R_{surf} [W·m^{-2}]	z_{inv} [m]	$\Delta\theta_{v,inv}$ [K·km^{-1}]	CTH_{max} [m]	CC [%]	CF_{base} [%]	CF_{inv} [%]	LWP [g·m^{-2}]	α [%]
DRY.unirad	264	2.7	6.60	29.8	2,165	5.5	5,850	9.1	3.4	1	10.23	4.9
WET.unirad	227	1.8	5.51	22.3	1,896	6.1	5,279	9.3	3.2	1.3	8.83	5.0
WET.homrad	202	1.5	4.79	13.4	1,959	12.7	2,381	12.4	3.3	3.7	8.93	6.4
WET.small	224	−1.8	4.32	1.2	2,431	17.5	2,627	12.2	3.4	2.2	11.08	6.4

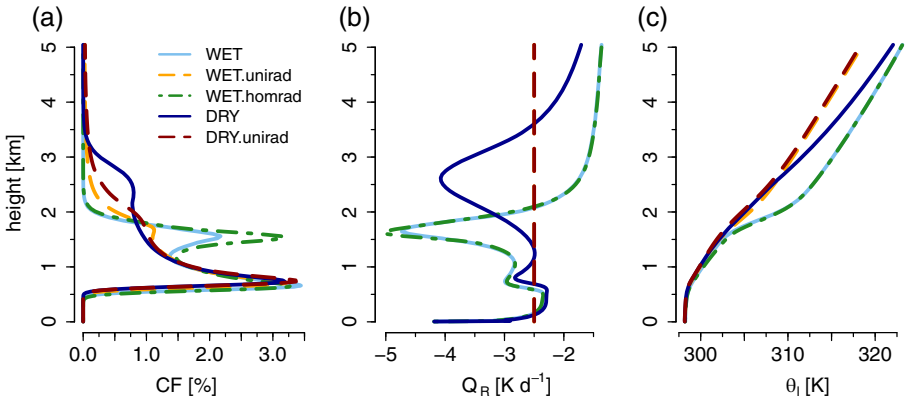

FIGURE 5 Domain-averaged profiles of (a) cloud fraction, (b) radiative heating tendency, and (c) liquid water potential temperature, for the *WET*, the *WET.unirad*, the *WET.homrad*, the *DRY*, and the *DRY.unirad* simulations

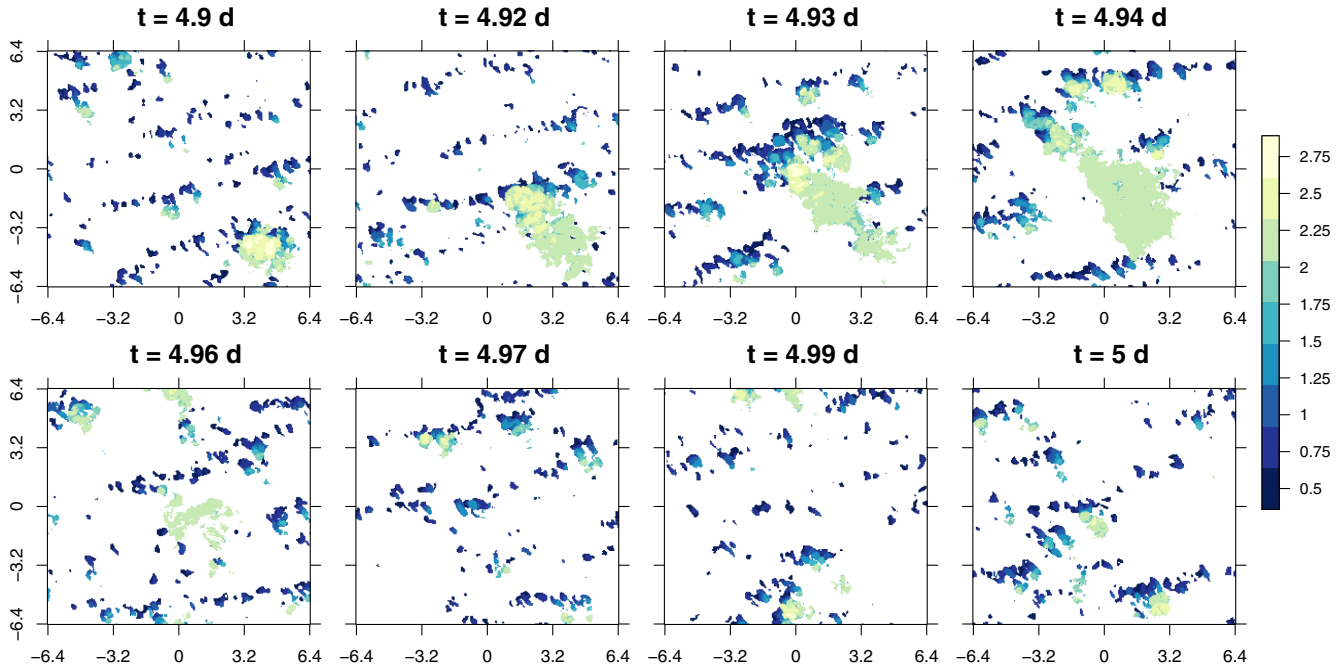

FIGURE 6 Horizontal cross-sections of cloud-top height (km) for the *WET.small* case at eight consecutive times starting after 4.9 days of the simulation. The snapshots are separated by 20 min (compared to 40 and 80 min separation in Figure 3 for the *WET* case)

the trade-wind layer structure (see also Vogel *et al.*, 2016). Figure 7c shows that the stability in the cloud layer is weaker and the inversion stronger in the *WET.small* case compared to the *WET* case. Also, the relative humidity in the cloud layer is enhanced in the *WET.small* case (Figure 7d). The stronger inversion is associated with a less rapidly deepening and less precipitating cloud field in the *WET.small* case in contrast to the *WET* case (not shown). Because precipitation eventually limits the deepening of the cloud layer (Stevens and Seifert, 2008; Bretherton *et al.*, 2013; Vogel *et al.*, 2016), the *WET.small* case ends up having a deeper cloud layer than the *WET* case (Figure 7c).

Surprisingly, the near-equilibrium cloud fraction profiles in Figure 7b show that both simulations produce the same amount of stratiform cloudiness. The cross-sections indicate that stratiform layers in the *WET.small* case form from detrainment of more isolated cumulus clouds rather than from large clusters as in the *WET* case (compare Figures 3a–c and 6). The 25% larger inversion strength and the 10% absolute increase in relative humidity in the *WET.small* case hence support stratiform cloudiness also in the absence of organized cloud clusters.

To investigate whether the two simulations have a different updraught structure, Figure 7f–h show cloud and cloud-core conditioned profiles of humidity, liquid water and vertical velocity. Core-conditioned averages refer to cloudy grid points with positive buoyancy compared to the slab-average (see dashed lines in Figure 7b for the core fractions). As expected from the smaller moisture variance, cloud and core regions in the small-domain *WET.small* case are drier than in

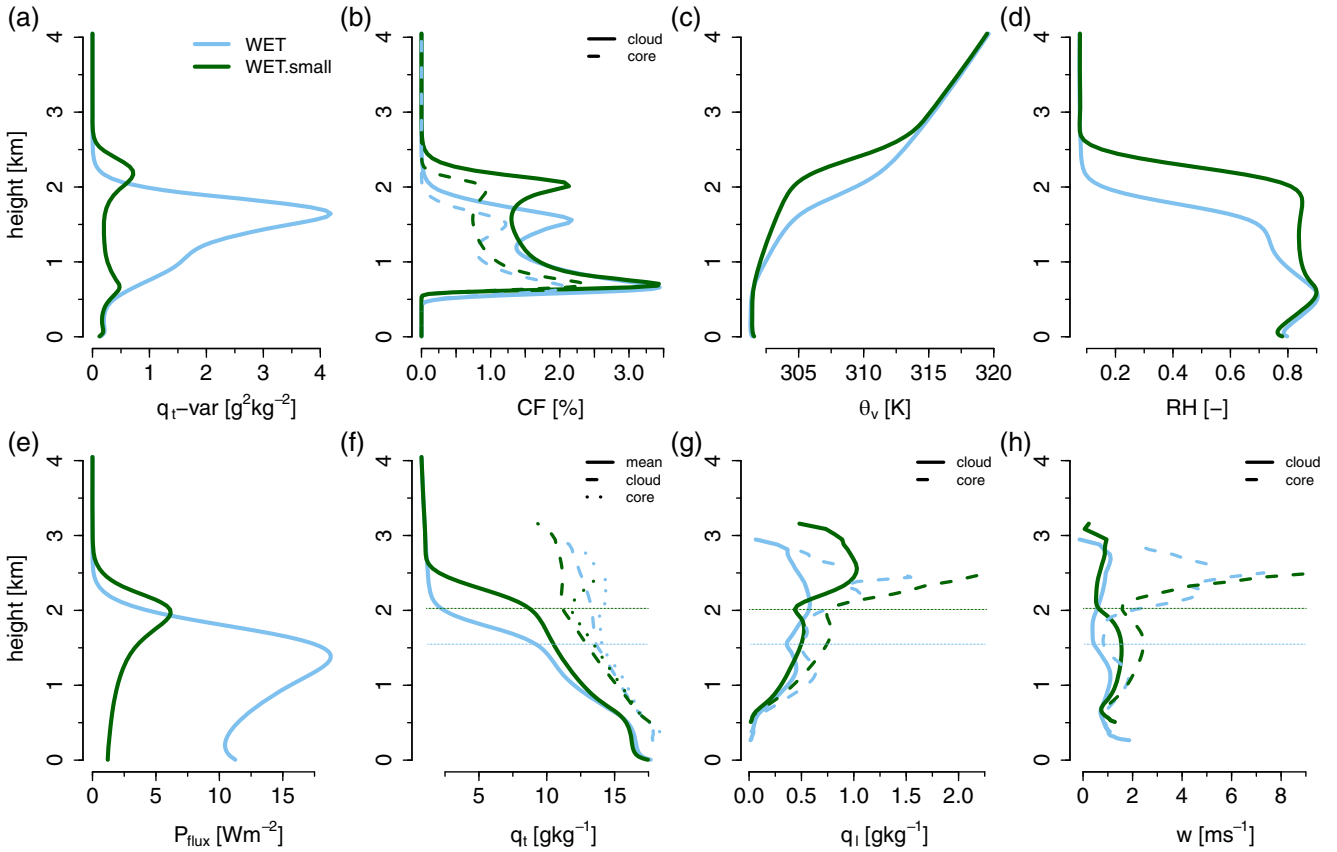

FIGURE 7 Domain-averaged profiles of (a) moisture variance, (b) cloud and core fraction, (c) virtual potential temperature, (d) relative humidity, (e) precipitation flux, and conditional cloud and core averages of (f) total humidity, (g) liquid water and (h) vertical velocity, for the *WET* and the *WET.small* case. Reference lines indicating the height of the inversion cloud maximum are added in (f–h)

the large-domain *WET* case. The cloud and core liquid water content in the *WET.small* case also increases less strongly with height, indicative of enhanced lateral entrainment drying compared to the *WET* case. However, the updraughts in the *WET.small* case are slightly more buoyant, and hence stronger than in the *WET* case, which is caused by the environment being colder on the small domain (Figure 7c). The interpretation of the conditional profiles well-above the inversion is difficult because of the small cloud and core fractions there.

Overall, the positive effects on stratiform cloudiness from the increase in inversion strength and updraught buoyancy in the absence of mesoscale organization seem to be compensated by the negative effects on the moisture and liquid-water content of updraughts, resulting in equal amounts of stratiform cloudiness for the two cases.

6 | SUMMARY AND CONCLUSIONS

We use large-eddy simulation (LES) to study the influence of the deepening and organization of shallow convection on stratiform cloudiness in the downstream trades. By performing LES with different large-scale forcings, radiation specifications and domain sizes, we isolate the influence of convective deepening, moisture–radiation interactions, and mesoscale organization on the stratiform cloudiness.

Figure 8 summarizes the main relationships between the inversion strength, cloudiness and the depth of convection found across the simulations. The inversion strength correlates with total cloud cover (Figure 8a), because cloud cover variations are mainly due to variations in cloud fraction near the inversion (Figure 8b), whereas variations near cloud base are less important (see Figure 1a or e.g. Nuijens *et al.*, 2014). The deepening of the cloud layer and the associated increase in precipitation are correlated with a reduction in inversion strength (Figure 8c,d). The simulations suggest that the details of how a specific change in the large-scale forcings deepens the cloud layer do not seem to matter much for the inversion strength and cloudiness. What matters most is the amount of deepening induced.

The three simulations departing from the linear relationship between inversion height and inversion strength in Figure 8c are the simulations using uniform prescribed radiation and the simulation on the small domain. The main conclusions of these sensitivity experiments with modified model set-ups are:

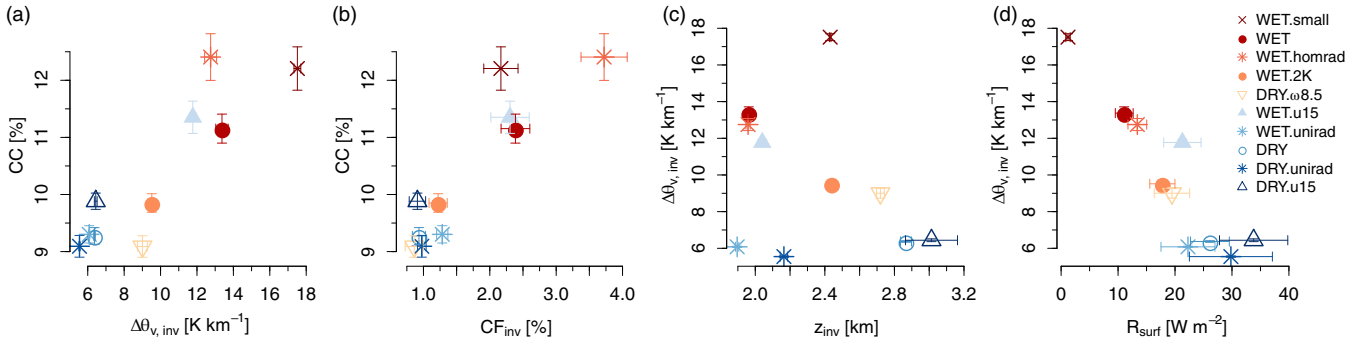

FIGURE 8 Scatterplots of cloud cover as a function of (a) inversion strength and (b) inversion cloudiness (defined as the cloud fraction maximum within 400 m below the inversion height), and inversion strength as a function of (c) inversion height and (d) surface rain rate. The symbols represent the mean and the whiskers represent the standard error ($\pm\sigma/n$, where n represents number of independent samples [every 4 h]) in the near-equilibrium regime of the simulations (see Table 1 for the averaging periods of individual simulations)

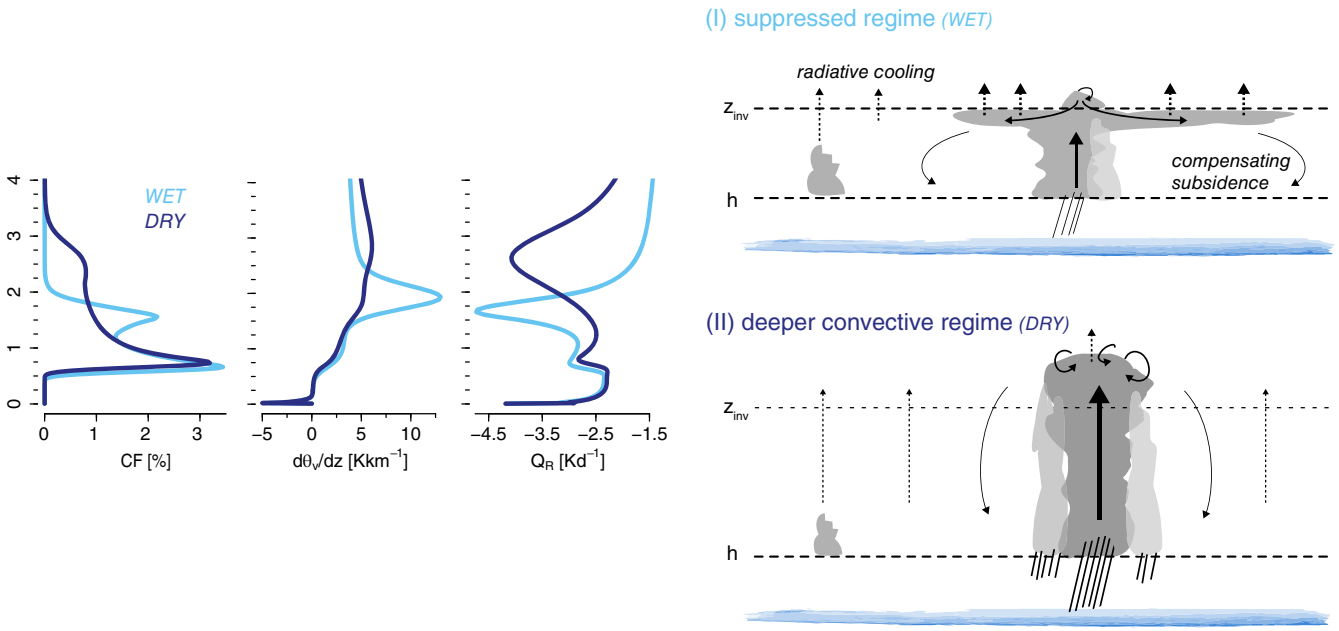

FIGURE 9 Schematic illustration of the main relationships between inversion strength, cloudiness and the depth of convection. Shown are also profiles of cloud fraction, stability and radiative heating tendency for the *WET* and the *DRY* simulations. *h* refers to the sub-cloud layer top

1 Interactive radiation is important to form strong inversions and stratiform cloudiness. Stronger radiative cooling from a larger moisture gradient across the inversion promotes larger cloudiness there, and vice versa, larger cloudiness there promotes stronger radiative cooling: a positive feedback (see also Stevens *et al.*, 2001; Lock, 2009).
2 Interactive radiation increases the sensitivity to the free-tropospheric humidity profile. Stronger radiative cooling in simulations with a drier free troposphere deepens convection, increases precipitation, and reduces stratiform cloudiness compared to simulations with a moister free troposphere.
3 The mesoscale organization of shallow convection in large-domain simulations has compensating positive effects (enhanced moisture transport related to a larger moisture variance) and negative effects (reduced inversion strength related to increased precipitation) on stratiform cloudiness.

The schematic in Figure 9 illustrates the main findings by distinguishing two regimes, a suppressed regime with stratiform cloudiness and a deeper convective regime without stratiform cloudiness. (I) In a more suppressed regime with a relatively shallow trade-wind layer (as represented by the *WET* simulation), organized cloud clusters transport a lot of moisture to the stable inversion and induce stratiform cloudiness, while strong radiative cooling maintains cloudiness and stabilizes the inversion. The occurrence of this regime may be related to the inversion forming below the height at which convection precipitates substantially, favouring its maintenance. (II) In a deeper convective regime that is more strongly forced (represented here by the *DRY* simulation), the

cloud layer is deeper, precipitation enhanced, and the inversion weaker. The deeper cloud clusters penetrate the inversion and either precipitate the moisture out or detrain it in the free troposphere, further weakening the inversion and inhibiting stratiform cloudiness.

The strong sensitivity of stratiform cloudiness to inversion height and strength suggested by the LES may help explain differences in the observed cloud profile between the winter and summer trades at Barbados. In winter, stratiform layers co-occur with slightly deeper trade cumuli (Nuijens *et al.*, 2014; Lamer *et al.*, 2015). But in summer, when the intertropical convergence zone is close and deep convection is more frequent, less stratiform cloudiness and weaker inversions are observed (Nuijens *et al.*, 2015b). The mean winter and summer trades are thus reminiscent of the suppressed and the deeper convective regime of Figure 9. In nature, there are also other factors influencing the inversion strength and stratiform cloudiness that are not considered in our LES, like the diurnal cycle of trade cumuli (Vial *et al.*, 2019). It is thus important to address the relationships found in the present study with observations, and with LES using more realistic forcings and boundary conditions, like the ICON-LEM (Large-Eddy Model configuration of the ICOsahedral Nonhydrostatic model) simulations over the tropical Atlantic of Klocke *et al.* (2017). Furthermore, the extent to which our findings are sensitive to the representation of microphysical processes merits further study (Stevens and Seifert, 2008; O *et al.*, 2018; Wood *et al.*, 2018).

Overall, the simulations show that the controls on the inversion strength in the downstream trades can be subtle, and the resulting response of stratiform cloudiness difficult to anticipate. Nevertheless, the simulations suggest a strong influence of the development of convection itself, particularly associated with the onset of precipitation and moisture–radiation interactions. This has important consequences for total cloud cover in this regime critical for climate sensitivity.

ACKNOWLEDGEMENTS

We thank Axel Seifert for advice concerning the interactive radiation implementation, and Marcus Klingebiel, Hauke Schulz, and two anonymous reviewers for constructive comments on an earlier version of this manuscript. Louise Nuijens wishes to acknowledge the opportunity to spend one year at MIT during this work through the Reimar Luest Stipendium and Max Kade Foundation Postdoctoral Research Grant. The UCLA LES model is distributed under the GNU General Public License and can be downloaded from https://github.com/uclales/uclales. The LES code, input files and analysis scripts are available on request from publications@mpimet.mpg.de. This work stems from the first author's doctoral research at the University of Hamburg.

ORCID

Raphaela Vogel https://orcid.org/0000-0002-8666-5147
Louise Nuijens https://orcid.org/0000-0003-0989-7443
Bjorn Stevens https://orcid.org/0000-0003-3795-0475

REFERENCES

Bellon, G. and Stevens, B. (2012) Using the sensitivity of large-eddy simulations to evaluate atmospheric boundary layer models. *Journal of the Atmospheric Sciences*, 69(5), 1582–1601. https://doi.org/10.1175/JAS-D-11-0160.1.

Bony, S. and Dufresne, J.L. (2005) Marine boundary layer clouds at the heart of tropical cloud feedback uncertainties in climate models. *Geophysical Research Letters*, 32(20), L20806. https://doi.org/10.1029/2005GL023851.

Boucher, O., Randall, D., Artaxo, P., Bretherton, C.S., Feingold, G., Forster, P., Kerminen, V.M., Kondo, Y., Liao, H., Lohmann, U., Rasch, P., Satheesh, S., Sherwood, S., Stevens, B. and Zhang, X. (2013) *Clouds and aerosols*. In *Climate Change 2013*. Cambridge and New York, NY: Cambridge University Press, pp. 571–658. https://doi.org/10.1017/CBO9781107415324.016.

Bretherton, C.S., Blossey, P.N. and Jones, C.R. (2013) Mechanisms of marine low cloud sensitivity to idealized climate perturbations: a single-LES exploration extending the CGILS cases. *Journal of Advances in Modeling Earth Systems*, 5(2), 316–337. https://doi.org/10.1002/jame.20019.

Bretherton, C.S., Peters, M.E. and Back, L.E. (2004) Relationships between water vapor path and precipitation over the tropical oceans. *Journal of Climate*, 17(7), 1517–1528. https://doi.org/10.1175/1520-0442(2004)017<1517:RBWVPA>2.0.CO;2.

Brueck, M., Nuijens, L. and Stevens, B. (2015) On the seasonal and synoptic time-scale variability of the North Atlantic trade wind region and its low-level clouds. *Journal of the Atmospheric Sciences*, 72(4), 1428–1446. https://doi.org/10.1175/JAS-D-14-0054.1.

Fu, Q. and Liou, K.N. (1992) On the correlated k-distribution method for radiative transfer in nonhomogeneous atmospheres. *Journal of the Atmospheric Sciences*, 49, 2139–2156.

Grabowski, W.W. and Moncrieff, M.W. (2004) Moisture–convection feedback in the Tropics. *Quarterly Journal of the Royal Meteorological Society*, 130(604), 3081–3104. https://doi.org/10.1256/qj.03.135.

Klocke, D., Brueck, M., Hohenegger, C. and Stevens, B. (2017) Rediscovery of the doldrums in storm-resolving simulations over the tropical Atlantic. *Nature Geoscience*, 10, 891–896. https://doi.org/10.1038/s41561-017-0005-4.

Lamer, K., Kollias, P. and Nuijens, L. (2015) Observations of the variability of shallow trade wind cumulus cloudiness and mass flux. *Journal of Geophysical Research: Atmospheres*, 120(12), 6161–6178. https://doi.org/10.1002/2014JD022950.

Lock, A.P. (2009) Factors influencing cloud area at the capping inversion for shallow cumulus clouds. *Quarterly Journal of the Royal Meteorological Society*, 135, 941–952. https://doi.org/10.1002/qj.424.

Medeiros, B. and Nuijens, L. (2016) Clouds at Barbados are representative of clouds across the trade wind regions in observations and climate models. *Proceedings of the National Academy of Sciences of the USA*, 113(22), E3062–E3070. https://doi.org/10.1073/pnas.1521494113.

Nuijens, L., Medeiros, B., Sandu, I. and Ahlgrimm, M. (2015a) The behavior of trade-wind cloudiness in observations and models: the major cloud components and their variability. *Journal of Advances in Modeling Earth Systems*, 7(2), 600–616. https://doi.org/10.1002/2014MS000390.

Nuijens, L., Medeiros, B., Sandu, I. and Ahlgrimm, M. (2015b) Observed and modeled patterns of covariability between low-level cloudiness and the structure of the trade-wind layer. *Journal of Advances in Modeling Earth Systems*, 7(4), 1741–1764. https://doi.org/10.1002/2015MS000483.

Nuijens, L., Serikov, I., Hirsch, L., Lonitz, K. and Stevens, B. (2014) The distribution and variability of low-level cloud in the North Atlantic trades. *Quarterly Journal of the Royal Meteorological Society*, 140(684), 2364–2374. https://doi.org/10.1002/qj.2307.

O, K.T., Wood, R. and Tseng, H.H. (2018) Deeper, precipitating PBLs associated with optically thin veil clouds in the Sc–Cu transition. *Geophysical Research Letters*, 45(10), 5177–5184. https://doi.org/10.1029/2018GL077084.

Pincus, R. and Stevens, B. (2009) Monte Carlo spectral integration: a consistent approximation for radiative transfer in large eddy simulations. *Journal of Advances in Modeling Earth Systems*, 1(1). https://doi.org/10.3894/JAMES.2009.1.1.

Savic-Jovcic, V. and Stevens, B. (2008) The structure and mesoscale organization of precipitating stratocumulus. *Journal of the Atmospheric Sciences*, 65(5), 1587–1605. https://doi.org/10.1175/2007JAS2456.1.

Seifert, A. and Beheng, K.D. (2001) A double-moment parameterization for simulating autoconversion, accretion and selfcollection. *Atmospheric Research*, 59–60, 265–281.

Seifert, A. and Beheng, K.D. (2006) A two-moment cloud microphysics parameterization for mixed-phase clouds. Part 1: Model description. *Meteorology and Atmospheric Physics*, 92(1–2), 45–66. https://doi.org/10.1007/s00703-005-0112-4.

Seifert, A. and Heus, T. (2013) Large-eddy simulation of organized precipitating trade wind cumulus clouds. *Atmospheric Chemistry and Physics*, 13(11), 5631–5645. https://doi.org/10.5194/acp-13-5631-2013.

Seifert, A., Heus, T., Pincus, R. and Stevens, B. (2015) Large-eddy simulation of the transient and near-equilibrium behavior of precipitating shallow convection. *Journal of Advances in Modeling Earth Systems*, 7(4), 1918–1937. https://doi.org/10.1002/2015MS000489.

Siebesma, A.P., Bretherton, C.S., Brown, A., Chlond, A., Cuxart, J., Duynkerke, P.G., Jiang, H., Khairoutdinov, M., Lewellen, D., Moeng, C.H., Sanchez, E., Stevens, B. and Stevens, D.E. (2003) A large eddy simulation intercomparison study of shallow cumulus convection. *Journal of the Atmospheric Sciences*, 60(10), 1201–1219. https://doi.org/10.1175/1520-0469(2003)60<1201:ALESIS>2.0.CO;2.

Stevens, B., Ackerman, A.S., Albrecht, B.A., Brown, A.R., Chlond, A., Cuxart, J., Duynkerke, P.G., Lewellen, D.C., Macvean, M.K., Neggers, R.A.J., Snchez, E., Siebesma, A.P. and Stevens, D.E. (2001) Simulations of trade wind cumuli under a strong inversion. *Journal of the Atmospheric Sciences*, 58(14), 1870–1891. https://doi.org/10.1175/1520-0469(2001)058<1870:SOTWCU>2.0.CO;2.

Stevens, B., Bony, S., Brogniez, H., Hentgen, L., Hohenegger, C., Kiemle, C., L'Ecuyer, T.S., Naumann, A.K., Schulz, H., Siebesma, P.A., Vial, J., Winker, D. and Zuidema, P. (2019) Sugar, gravel, fish and flowers: mesoscale cloud patterns in the trade winds. *Quarterly Journal of the Royal Meteorological Society* (accepted). doi:10.1002/qj.3662. https://rmets.onlinelibrary.wiley.com/doi/abs/10.1002/qj.3662.

Stevens, B., Cotton, W.R., Feingold, G. and Moeng, C.H. (1998) Large-eddy simulations of strongly precipitating, shallow, stratocumulus-topped boundary layers. *Journal of the Atmospheric Sciences*, 55(24), 3616–3638. https://doi.org/10.1175/1520-0469(1998)055<3616:LESOSP>2.0.CO;2.

Stevens, B., Moeng, C.H., Ackerman, A., Bretherton, C., Chlond, A., de Roode, S., Edwards, J., Golaz, J.C., Jiang, H., Khairoutdinov, M., Kirkpatrick, M., Lewellen, D., Lock, A., Müller, F., Stevens, D., Whelan, E. and Zhu, P. (2005) Evaluation of large-eddy simulations via observations of nocturnal marine stratocumulus. *Monthly Weather Review*, 133(6), 1443–1462. https://doi.org/10.1175/MWR2930.1.

Stevens, B. and Seifert, A. (2008) Understanding macrophysical outcomes of microphysical choices in simulations of shallow cumulus convection. *Journal of the Meteorological Society of Japan*, 86A, 143–162. https://doi.org/10.2151/jmsj.86A.143.

Vial, J., Dufresne, J.L. and Bony, S. (2013) On the interpretation of inter-model spread in CMIP5 climate sensitivity estimates. *Climate Dynamics*, 41, 3339–3362. https://doi.org/10.1007/s00382-013-1725-9.

Vial, J., Vogel, R., Bony, S., Stevens, B., Winker, D.M., Cai, X., Hohenegger, C., Naumann, A.K. and Brogniez, H. (2019) A new look at the daily cycle of tradewind cumuli. *Journal of Advances in Modeling Earth Systems*, 11. https://doi.org/10.1029/2019MS001746.

Vogel, R., Nuijens, L. and Stevens, B. (2016) The role of precipitation and spatial organization in the response of trade-wind clouds to warming. *Journal of Advances in Modeling Earth Systems*, 8(2), 843–862. https://doi.org/10.1002/2015MS000568.

Wood, R., O, K.-T., Bretherton, C.S., Mohrmann, J., Albrecht, B.A., Zuidema, P., Ghate, V., Schwartz, C., Eloranta, E., Glienke, S., Shaw, R.A., Fugal, J. and Minnis, P. (2018) Ultraclean layers and optically thin clouds in the stratocumulus-to-cumulus transition. Part I: Observations. *Journal of the Atmospheric Sciences*, 75(5), 1631–1652. https://doi.org/10.1175/JAS-D-17-0213.1.

Wyant, M.C., Bretherton, C.S., Rand, H.A. and Stevens, D.E. (1997) Numerical simulations and a conceptual model of the stratocumulus to trade cumulus transition. *Journal of the Atmospheric Sciences*, 54(1), 168–192. https://doi.org/10.1175/1520-0469(1997)054<0168:NSAACM>2.0.CO;2.

Yanai, M., Esbensen, S. and Chu, J.H. (1973) Determination of bulk properties of tropical cloud clusters from large-scale heat and moisture budgets. *Journal of the Atmospheric Sciences*, 30, 611–627.

Zhang, Y., Stevens, B. and Ghil, M. (2005) On the diurnal cycle and susceptibility to aerosol concentration in a stratocumulus-topped mixed layer. *Quarterly Journal of the Royal Meteorological Society*, 131(608), 1567–1583. https://doi.org/10.1256/qj.04.103.

How to cite this article: Vogel R, Nuijens L, Stevens B. Influence of deepening and mesoscale organization of shallow convection on stratiform cloudiness in the downstream trades. *Q J R Meteorol Soc*. 2019;1–12. https://doi.org/10.1002/qj.3664